Dissimilar diffusion welding of some equiatomic FCC-structured CoCrFeNi-based binary and multi-component alloys to 316 L stainless steel.

Olushola Bamidele Nenuwa, Léo Thiercelin, Laurent Peltier, Eric Fleury, Nathalie Siredey-Schwaller, Adil Benaarbia

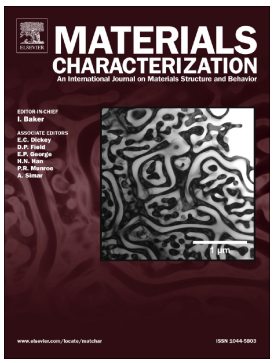

Dissimilar diffusion welding of some equiatomic FCC-structured CoCrFeNi-based binary and multi-component alloys to 316L stainless steel

Olushola Bamidele Nenuwa, Léo Thiercelin, Laurent Peltier, Eric Fleury, Nathalie Siredey-Schwaller, Adil Benaarbia

PII: S1044-5803(25)00462-0

DOI: https://doi.org/10.1016/j.matchar.2025.115173

Reference: MTL 115173

To appear in: *Materials Characterization*

Received date: 9 October 2024

Revised date: 4 May 2025

Accepted date: 13 May 2025

Please cite this article as: O.B. Nenuwa, L. Thiercelin, L. Peltier, et al., Dissimilar diffusion welding of some equiatomic FCC-structured CoCrFeNi-based binary and multi-component alloys to 316L stainless steel, *Materials Characterization* (2024), https://doi.org/10.1016/j.matchar.2025.115173

Dissimilar diffusion welding of some equiatomic FCC-structured CoCrFeNi-based binary and multi-component alloys to 316L stainless steel

Olushola Bamidele Nenuwa[a,c], Léo Thiercelin[a], Laurent Peltier[a], Eric Fleury[a], Nathalie Siredey-Schwaller[a], Adil Benaarbia[a,b*]

[a]Arts et Métiers Institute of Technology, CNRS, Université de Lorraine, LEM3-UMR 7239, F-57000, Metz, France
[b]Univ. Lille, CNRS, INRAE, Centrale Lille, UMR 8207 – UMET – Unité des Matériaux et Transformations, F-59000 Lille, France
[c]Department of Mineral & Petroleum Resources Engineering, Federal Polytechnic, P.M.B. 5351, Ado-Ekiti, Nigeria
*Corresponding author's email: adil.benaarbia@centralelille.fr

Abstract

This investigation was carried out to assess the joint integrity of dissimilar diffusion welding of some equiatomic binary and multi-component alloys (MCAs), viz. CoNi, CoCrNi and CoCrFeNi, to 316L stainless steel (SS316L). The microstructures and chemical composition gradients across the bond interfaces were examined by a Scanning Electron Microscope (SEM) equipped with an Energy Dispersive Spectrometer (EDS), Electron Back Scattered Diffraction (EBSD) and X-ray Diffraction (XRD) analyses, while the mechanical properties were assessed by shear tests. The binary and multi-component alloys were successfully joined to SS316L with low interfacial defects and without any compositional segregation or formation of secondary intermetallic compounds at the bond interfaces. The shear tests revealed that SS316L-CoCrNi and SS316L-CoCrFeNi joints offered good shear strength and ductility which are comparable to that of SS316L similar joints, while SS316L-CoNi joint displayed the least mechanical performances.

Keywords:

Chemical gradients, Diffusion welding, Microstructural Characterization, Multi-component alloys, Shear properties, Stainless steel.

1. Introduction

Multi-component alloys (MCAs) are well known for their good corrosion resistance, radiation damage resistance, fatigue resistance, fracture toughness and strength [1], [2] and could be used for different applications in the nuclear, marine, automotive, aerospace, communication, chemical and petroleum industries [3], [4]. The CoNi binary systems were found to exhibit high strength and ductility [5]. The equiatomic CoCrNi displayed exceptional strength-toughness properties and damage tolerance at cryogenic temperatures [6]. It has been reported that the equiatomic CoCrFeNi has higher mechanical properties and strain-hardening rates compared to the CoCrFeMnNi high entropy alloy [7]. Therefore, due to the unique properties of most of the multi-component alloys, they can replace conventional alloys in structural applications or components operating under extreme environments. Dissimilar welding of MCAs with conventional alloys is now gaining more attention because it can offer better manufacturing economy, design flexibility and performance enhancements [8], [9]. The 316L stainless steel (SS316L) is a low-carbon chromium-nickel-molybdenum austenitic stainless steel that has a relatively good property-over-cost ratio and with near-identical properties to the above mentioned MCAs, especially in terms of corrosion resistance and strength [10], [11]. The MCAs have some superior properties that make them preferred materials for application in cryogenic conditions. For instance, both the tensile strength and fracture toughness of equiatomic CoCrNi increase with decreasing temperature whereas for the SS316L, the tensile strength increases with decreasing temperature but the fracture toughness decreases with decreasing temperature [12]. Based on cost considerations, MCAs are more likely to be used to partially replace SS316L in critical parts of structural applications

exposed to severe conditions. Hence, it is important to understand the weldability of some equiatomic single-phase CoNi, CoCrNi, and CoCrFeNi alloys with 316L stainless steel to assure product reliability [13], [14], [15].

Although, several works have been conducted on similar welding of MCAs, dissimilar welding of these alloys with stainless steels or other materials with equal interest is currently being explored worldwide. For instance, laser welding of rolled CoCrFeMnNi HEA to 316 stainless steel was performed by Oliveira et al. [16]. The microstructure in the fusion zone was found to be composed of a single FCC phase with a higher hardness value compared to the SS316. These laser welded joints displayed a tensile strength lower than that of HEA base metal but higher than the SS316. Another study [17] examined dissimilar weld joints of $Al_{0.1}$CoCrFeNi HEA and AISI304 stainless steel using tungsten inert gas welding, the joint presented higher tensile strength than the HEA, making it suitable for structural applications. Dissimilar laser welding of CoCrNi medium entropy alloy and 301L stainless steel has been conducted[15], and equiatomic CoCrFeMnNi was also laser welded to duplex stainless steel [18]. These two studies reported that the fusion zones were composed of FCC single-phase.

Fusion-based dissimilar welding may not be suitable for joining some advanced materials because of the inherent residual stresses and possible distortion as well as the potential formation of detrimental phases that can form during the mixing and solidification of the two base materials [19], [20]. Diffusion welding (DFW) is an alternative solid-state joining process with the advantage of being applied at temperatures lower than the melting point minimizing welding distortion and keeping good material properties. This technique is widely used in aerospace, nuclear, electronics, and manufacturing industries [20], [21], [22] and could be

extended to the petroleum industries [23]. There have been reports on similar diffusion welding of austenitic stainless steel. Vacuum diffusion-bonded SS316L joints were conducted at a temperature of 1100°C, pressure of 10 MPa and holding time of 3 h [24]. No obvious bonding line was noticed on the interface but a few scattered microvoids, the tensile test revealed a decrease in ductility of the joint due to serious grain coarsening. A study by Mateus et al. (2017) examined the microstructural and mechanical properties of diffusion-bonded 316L stainless steel at different bonding temperatures, pressure and time. The bond quality was observed to be mostly influenced by the temperature as it increases the mass transport. Bonding at a temperature of 1040°C yielded the best results within the investigated set of parameters [25]. Diffusion welding has been adopted for joining 316L stainless steel to 4J29 Kovar alloy using a fine sheet of pure nickel as an interlayer [26], and for the welding of 316L stainless steel to 4J29 Kovar alloy using pure cobalt as an interlayer [27]. Recently, diffusion welding of multi-component alloys has been successfully carried out in the case of joining CoCrFeMnNi to pure copper [28] and bonding CoCrNi-based medium entropy alloy to the DD5 Ni-based single-crystal superalloy [29]. The effect of bonding temperature and time on the diffusion welding of CoCrNi to 304 stainless steel was also investigated [30], [31]. The authors reported that the weld discontinuities observed for welding temperatures below 1050°C and time duration below 3 hours were suppressed when these process parameters were increased. The frequency of Intermetallic carbide (IMC) that could also be formed along the bond interface was found to be reduced when the bonding temperature and time were increased. Spark plasma sintering was adopted for carrying out diffusion bonding of equiatomic CoCrNi-based concentrated solid solution alloys to SS316L at different bonding temperatures [32]. It was observed that increasing the bonding temperature led to an increase in the tensile strength of the joints, and for a welding time of 1 hour, the optimal

bonding temperature for all the joints was found to be about 80% of the melting point of base alloy having the lowest melting point.

Dissimilar diffusion welding may induce residual stress at the bond interface due to differences in the coefficient of thermal expansion of both materials which could lead to local plastic deformation and/or the formation of micro-cracks. New phases may occur at the bond region which are different from those of the parent metals. The joint might suffer a premature failure particularly when brittle intermetallic compounds form in the vicinity of the bond interface. Research on dissimilar diffusion welding of MCA-type materials especially with austenitic stainless steels is still very scarce hence, work focused on understanding the weldability of these alloys should get more attention. To the authors' knowledge, no study has been conducted on the diffusion welding of SS316L and the equiatomic FCC structured binary subsystem like CoNi alloy. None of the previous authors have compared the quality of SS316L-MCA diffusion welded joints with that of SS316L similar joints. The chemical complexity of MCAs has been reported to have a decisive influence on some thermophysical properties [33]. Hence, investigating the effect of the chemical composition of multi-component alloys when diffusion welded with SS316L is essential.

The main goal of this study was to investigate the feasibility of diffusion welding of some equiatomic FCC-structured CoCrFeNi-based alloys and SS316L using multiscale characterization techniques and mechanical shear tests. Equiatomic FCC-structured binary, ternary, and quaternary systems (CoNi, CoCrNi and CoCrFeNi) were elaborated and joined to the 316L stainless steel by diffusion welding under the same processing parameters. Similar diffusion welding of SS316L was also carried out to serve as a reference. The microstructures,

diffusion mechanisms, and mechanical properties of the welded assemblies were examined using a Scanning Electron Microscope equipped with an Energy Dispersive Spectrometer (SEM-EDS), Electron Back-Scattered Diffraction (EBSD) analysis and X-ray Diffraction (XRD) and shear tests. The diffusion chemical profiles were analysed to establish the diffusion zones and to determine the diffusion coefficients of the elements across the interfaces of the various assemblies. The Fick's second law of diffusion was used to compute the diffusion coefficients based on the finite difference method. In comparison to classical analysis, values of the diffusion coefficients were computed for each element in the parent materials on both sides of the diffusion joint.

The paper is outlined as follows: Section 2 presents the procedures for elaboration of the multi-component alloys, diffusion welding, microstructural characterization (SEM-EDS, EBSD and XRD techniques) and the shear tests. Section 3 presents the results obtained which include microstructures of parent samples by SEM, EBSD and XRD, microstructures of welded samples by SEM images and EBSD maps, chemical composition analyses of welded samples by EDS analysis, diffusion coefficients calculations of the major elements, shear properties of welded samples, fractography and XRD analyses of the ruptured surfaces. Section 4 is devoted to the global discussion of the results obtained while the last section presents the conclusions derived from the study.

2. Experimental procedures

2.1 Elaboration of multi-component alloys

Ingots weighing 150g of the equiatomic CoNi, CoCrNi and CoCrFeNi alloys were produced by vacuum induction melting of pure elements (purity ≥ 99.9 wt%) using a water-cooled copper

crucible. The vacuum induction furnace operating under a high-purity argon (Ar) protective atmosphere prevented elemental oxidation. The ingots were remelted five times to improve the compositional homogeneity before drop casting into moulds to produce parallelepipedic ingots with dimensions of 20 mm × 20 mm × 27 mm. The ingots were further homogenized by heat treatment at a temperature of 1200°C for 24 h of soaking time and then cooled by water quenching. Finally, the MCA samples were cut into cubes of 5 x 5 x 5 mm^3 dimensions for the diffusion welding experiment.

2.2 Diffusion welding

Dissimilar diffusion welding was conducted between the MCAs and a commercially sourced SS316L austenitic stainless steel plate of 10 mm thickness with chemical composition as verified by the spark optical emission spectrometer presented in Table 1. The other elements in SS316L are P (0.03 wt.%), S (0.003 wt.%), Ti (0.007 wt.%), V (0.07 wt.%), N (0.06 wt.%), W (0.06 wt.%). The SS316L which had a thermo-mechanical history of hot rolling, solution annealing and water quenching. All the heat-treated MCA samples were cut with the Struers Secotom-15 cutting machine according to the dimensions illustrated in Fig. 1. The samples to be diffusion welded were ground and polished to obtain mirror-like surfaces and properly cleaned with ethanol to remove contamination from the faying surfaces. The SS316L samples were polished perpendicularly to the normal direction (ND) and assembled with the MCAs as shown in Fig. 1(c), the assembled sample was then placed inside the diffusion welding set-up as illustrated in Fig. 2.

Table 1. The chemical composition of main elements in 316L stainless steel (wt.%).

Fe	C	Si	Mn	Cr	Mo	Ni	Co	Cu
Bal.	0.02	0.34	1.38	16.70	2.00	10.00	0.16	0.37

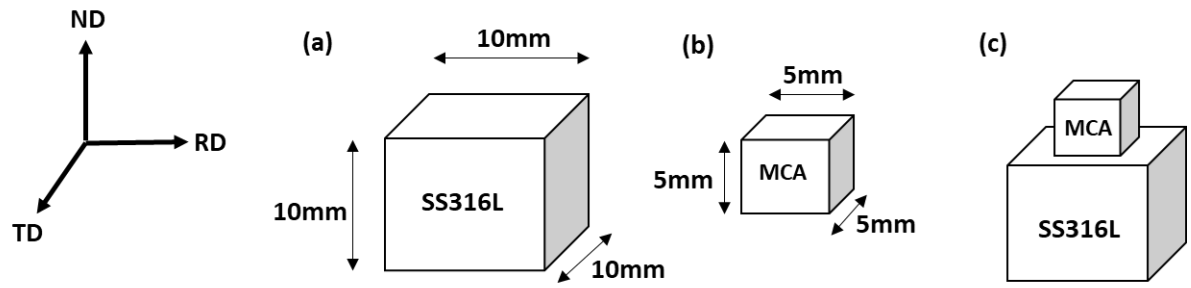

Fig. 1. Schematic illustration of the as-prepared samples (ND - Normal direction, RD – Rolling direction, TD – Traverse direction), (a) as-prepared 316L stainless steel sample, (b) as-prepared multi-component alloy sample, (c) diffusion welded assembly of SS316L and MCA.

Diffusion welding was conducted by loading the assembled sample under a compressive pressure of 5 MPa with the aid of the Zwick Roell Z050 uniaxial testing machine to ensure tight contact between the two samples (Fig. (2b)). The mounted diffusion welding set-up was then placed inside a furnace (Fig. (2c)) in which the environment was conditioned with argon gas after achieving secondary vacuum. The heating rate was set at 15°C/min to attain the holding temperature of 1075°C which was maintained for an hour for all the samples to be welded. Then, the furnace was switched off to allow the welded sample to cool to room temperature inside the furnace. By following similar procedures, the binary, ternary, and quaternary alloys were all welded to 316L stainless steel. Similar welding with SS316L was also conducted in similar conditions to serve as a reference. The processing parameters were set based on previous successful diffusion welding of 304 stainless steel and CoCrNi-based medium entropy alloy reported by Samiuddin and colleagues [30]. The welding temperature adopted was about 0.8 T_m (where T_m is the melting temperature in degrees Kelvin of the material having the lowest melting point, i.e., here the SS316L). The melting temperatures of

CoNi, CoCrNi, CoCrFeNi and SS316L are 1462°C, 1417°C, 1422°C and 1405°C respectively [10], [34], [35].

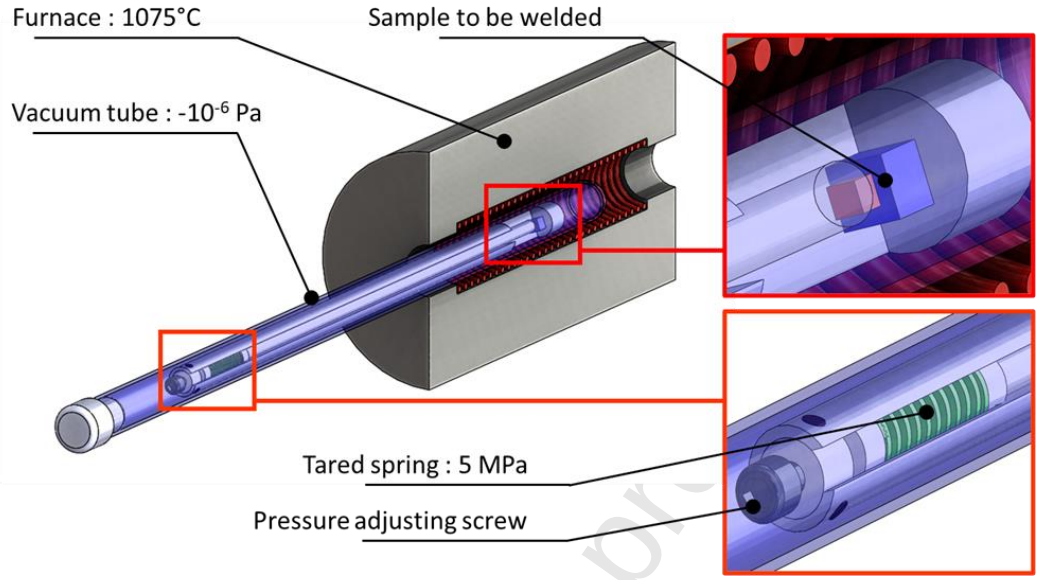

Fig. 2. Home-made diffusion welding set-up showing the various components of the welding bench.

2.3 Microstructural examination by SEM-EDS, EBSD and XRD analyses

All samples were prepared by the conventional metallographic sample preparation procedures. The samples were ground on silicon carbide abrasive paper of 15µm and polished with DiaPro 9 µm and 3 µm diamond suspensions and colloidal silica suspension to obtain a mirror-like surface. The microstructures of the samples were examined in a Zeiss Supra 40 scanning electron microscope (SEM) equipped with a Bruker X Flash 6/30 detector using the EDS technique for the chemical composition analyses. The composition was quantitatively measured at 15kV using the standards of pure Fe, Mn, Mo, Cr, Co, Ni and Si. After diffusion welding of the SS316L with the three different equatomic MCAs (CoNi, CoCrNi and CoCrFeNi), the welded assemblies followed the same metallographic preparation techniques. The bond interfaces revealed were similarly examined with the SEM-EDS machine. An image analysis

software (ImageJ 1.54d) was used for microstructural quantitative measurements based on standard test methods for determining average grain size using the standard ASTM E112. The electron backscattered diffraction (EBSD) analyses of the welded samples were conducted with the JEOL F100 scanning electron microscope equipped with Oxford Instruments EBSD detector. The step size of the low magnification maps was 1 µm while step sizes of 0.5 µm and 0.1 µm were selected for maps with higher magnification. The EBSD data was post-processed with the AZtecCrystal software to generate phase maps which were used for further examination of the microstructural evolution and grain boundary diffusion of the welded samples. The phases in the SS316L, heat-treated MCAs and fractured welded samples were investigated with the D8 Advance X-ray diffractometer (XRD) equipped with a Co anode (λ = 1.7903 Å) using a step size of 1°/s.

2.4 Mechanical testing of welded joints

The mechanical behaviour of the diffusion welded joints was assessed by conducting shear tests. The specimen for this test was prepared from cubes obtained from the two parent materials (Fig. 3(a)). The loading of the sample and the fixture is schematically shown in Fig. 3(b) and 3(c). The test was conducted using the Zwick Roell Z050 uniaxial testing machine at a strain rate of 0.5mm/min. Load was applied to the sample until fracture occurred. The bond shear strength, τ is defined as the ratio of failure load, F to the entire bonded area, A measured with the post-mortem sample. After the fracture, XRD and scanning electron microscopy equipped with an energy dispersive spectrometer (SEM-EDS) were used to assess the ruptured surfaces.

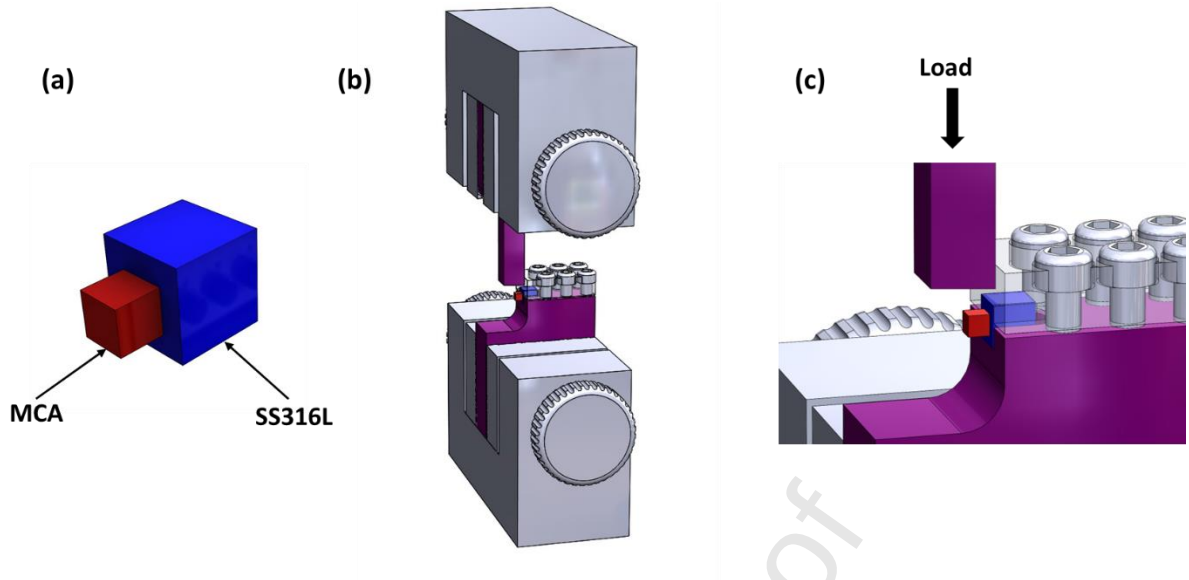

Fig. 3. Schematic illustration of the shear test set-up, a) test specimen, b) execution of shear test on the diffusion welded sample, c) closer view of the shear test set-up

3. Results

3.1 Microstructures of the parent samples

3.1.1 Microstructures of stainless steel

The micrograph produced in the secondary electrons mode of the SEM for SS316L is presented in Fig. 4(a) while Fig. 5 is the EBSD orientation map showing grain size distribution. Equiaxed grains and several twinnings are revealed in the as-received SS316L microstructure having an average grain size of 11.8 ± 1.3 µm. SS316L is a material with low stacking fault energy [36], therefore it is expected that its thermal history of solution heat treatment would have introduced several annealing twins as observed in the microstructure. To understand the grain growth kinetics of SS316L, the as-received sample was exposed to a temperature of 1075°C for 1 hour without loading and cooled in the furnace. Homogeneous grain growth was observed within the microstructure (Fig. (4b)) and the size of the new grains formed was 85.8 ± 12 µm which is about 7 times larger than that of the as-received SS316L sample.

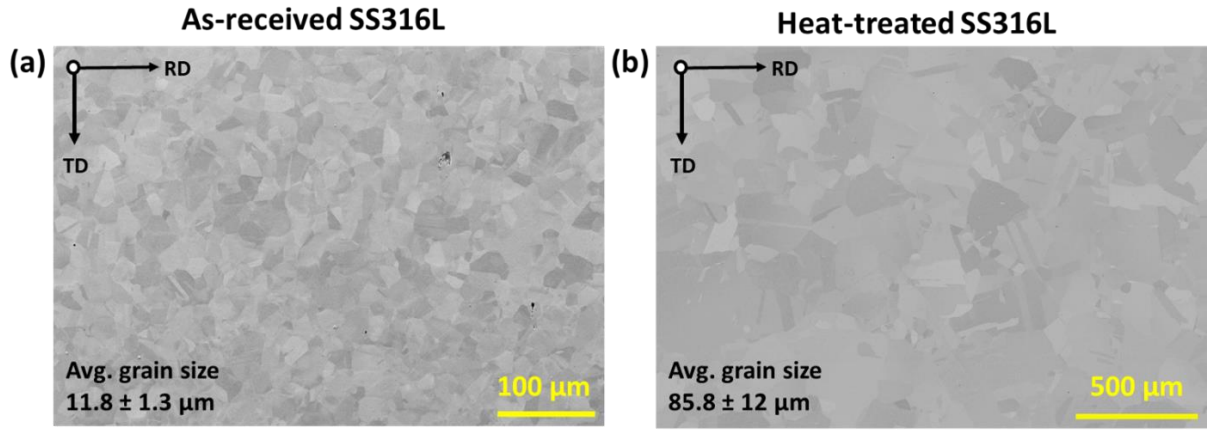

Fig. 4. Microstructure of SS316L sample taken perpendicularly to the normal direction (ND) (a) as-received SS316L (b) as-received SS316L heat treated at 1075°C for 1 hr and cooled in the furnace (under the same condition as the welded samples but without compressive loading).

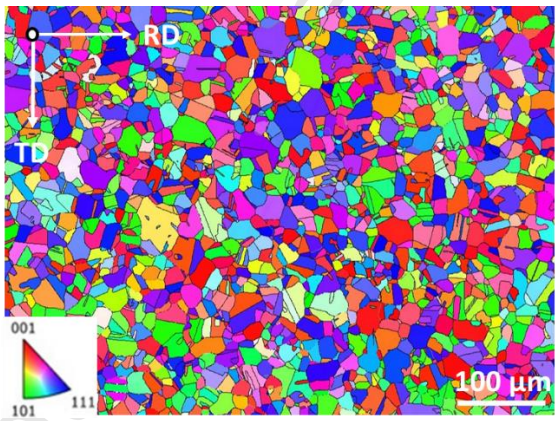

Figure 5. EBSD orientation maps of the as-received SS316L sample with inverse pole figures (IPF) as inset. (Fraction of LAGB (2° ≤ θ ≥ 10°) = 1.28% and Fraction of HAGB (θ >10°) = 98.7%).

3.1.2 Microstructures of the multi-component alloys

Fig. 6a – c shows the SEM microstructures of the multi-component alloys observed in secondary electron mode. The heat-treated CoNi, CoCrNi and CoCrFeNi MCA alloys have average grain sizes of 98.6 ± 8.8 µm, 84.6 ± 14.7 µm and 80.6 ± 11.3 µm respectively which is about 7 - 8 times greater than that of the as-received SS316L. It can be deduced from the

microstructural evolution of the MCAs that as the number of elements in the MCAs increased, the grain size became smaller. This trend was similarly observed in a previous study [32], and it was attributed to higher dislocation density as the number of components increased, which tends to retard the grain growth kinetics.

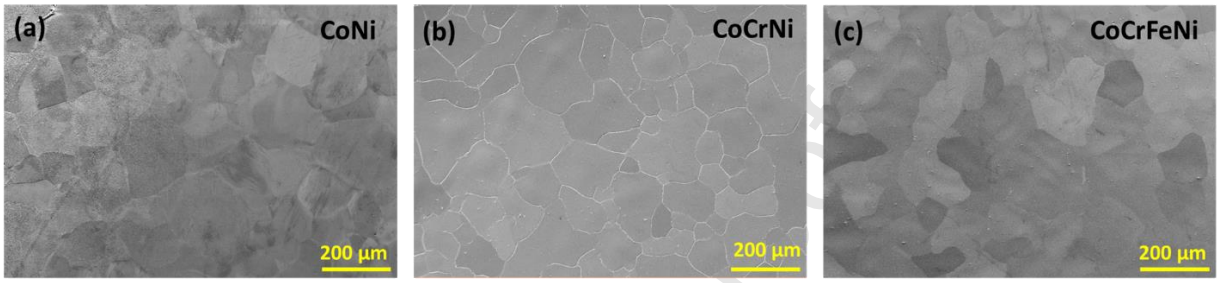

Fig. 6. SEM micrographs of equiatomic MCAs heat-treated at a temperature of 1200°C for 24 h and cooled by water quenching, (a) CoNi with an average grain size of 98.6 ±8.8 µm, (b) CoCrNi with an average grain size of 84.6 ±14.7 µm, (c) CoCrFeNi with an average grain size of 80.6 ± 11.3 µm

3.1.3 X-ray diffraction patterns of parent samples

Fig. 7 shows the X-ray diffraction patterns of the parent alloys (SS316L, CoNi, CoCrNi and CoCrFeNi). Only the three peaks corresponding to {111}, {200} and {220} family planes are noticed in all the patterns which are characteristics of a single-face cubic-centred (FCC) crystal structure. For SS316L, the austenite is the dominant FCC phase and the relative height of the intensity of (111) and (200) peaks suggests the presence of a moderate crystalline texture. The values of the lattice parameter, “a” for SS316L is 3.601 ± 0.002 Å, the values for the MCAs are 3.538 ± 0.001 Å, 3.571 ± 0.004 Å and 3.577 ± 0.003 Å for CoNi, CoCrNi and CoCrFeNi alloys respectively. It is observed that as the number of constituent elements in the MCAs increased, the values of the lattice parameter also increased. These results show that increasing the

number of constituent elements in the multi-component alloys would lead to gradual lattice expansion as already observed in a previous study [37].

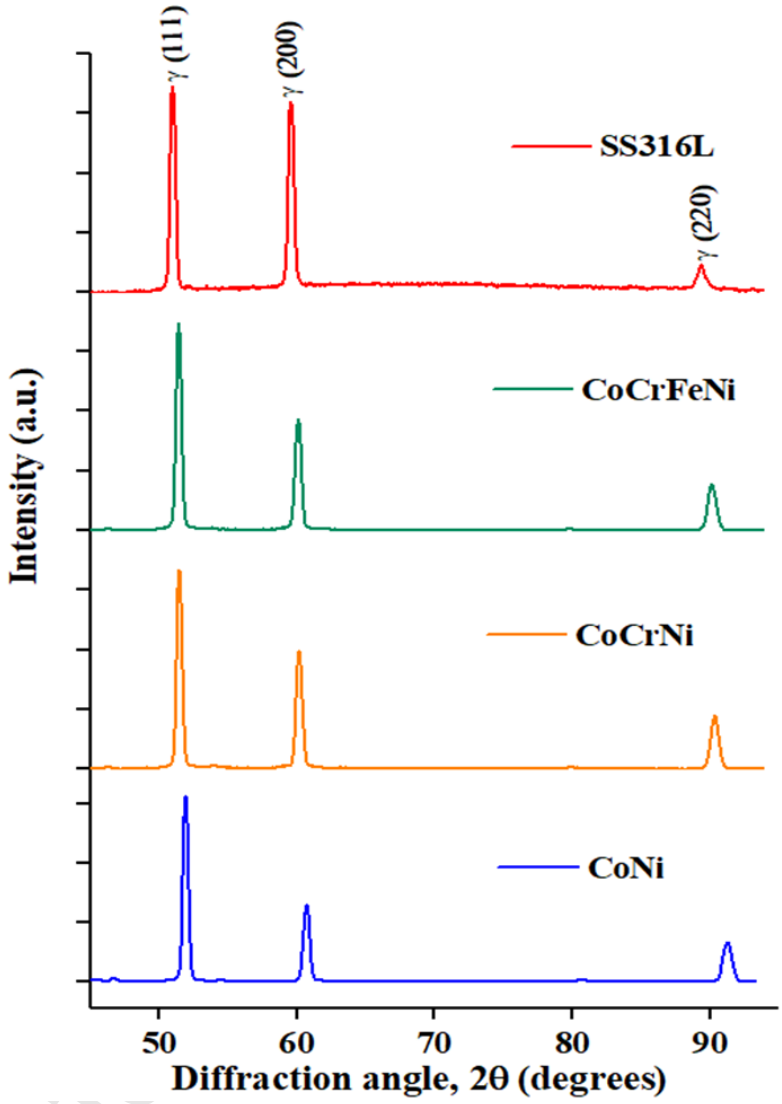

Fig. 7. XRD patterns of the parent materials: commercial SS316L and heat-treated MCA samples.

3.2 Microstructural features of the welded samples

3.2.1 SEM microstructural examination of welded joints

The microstructural examination provides a qualitative and quantitative evaluation of the diffusion welded samples. Fig. 8 presents the microstructures of the diffusion welded joints

as revealed by SEM operated in the back-scattered electron (BSE) mode. The associated grain distributions measured by ImageJ software are given in Table 2. The SEM maps of the similar diffusion SS316L welded sample shown in Fig. 8(a – b), reveal a good-quality joint without interfacial pores and few microvoids. The bond interface was less visible due to the material continuity resulting from grain growth across the bond interface. Annealing twins were detected and grain growth took place across the entire microstructure. The average size of the new grains formed in SS316L was 78.6 ± 16.5 µm which is about the same size or slightly smaller than the grain size observed when the as-received SS316L was heat-treated under similar temperature conditions but without any compressive stress (Fig. (4b)).

The BSE micrographs of the SS316L-CoNi joint at low and high magnification are presented in Fig. 8(c – d). The two materials were well joined with few interfacial pores and microvoids only noticeable at high magnification (Fig. (8d)), the average size of the interfacial pore being about 0.9 ± 0.2 µm. The microvoids which are randomly located around the CoNi alloy microstructure may have been introduced during the casting of the material. A diffusion zone was formed near the bond interface due to the mutual diffusion of elements during the bonding process. Another prominent feature is the coarsening of the SS316L grains near the bond interface. The average size of coarse SS316L grains is 77.4 ± 15.2 µm which is almost similar to the grain size of the SS316L after annealing at the same temperature (Fig. (4b)). The width of the region in which grain coarsening could be observed and highlighted by the yellow dashed line in Fig. 8(c) from the bond interface is about 645.6 ± 43 µm. Beyond this region, the average size of the SS316L fine grains was 20.59 ± 13.56 µm. However, the grains of the CoNi alloy after diffusion welding did not change significantly when compared with that of the as-fabricated CoNi alloy. As the MCAs were subjected to heat treatment at a temperature

of 1200°C for 24 hours, the welding temperature of 1075°C for 1 hr did not cause major microstructural evolution of the CoNi alloy.

The BSE micrographs for the joint between SS316L and CoCrNi are shown in Fig. 8(e – f). Tiny interfacial pores and microvoids were also found in the joint at high magnification as shown in Fig. 8(e). The average size of these interfacial pores is about 0.4 ± 0.2 μm which is smaller than those noticed in the SS316L-CoNi joint. Grain coarsening of SS316L was also observed with the average size of coarse SS316L grains being 49.7 ± 11.9 μm, which is smaller than the grain size for the SS316L annealed in similar conditions. The distance from the bond interface to the grain coarsening boundary is 256.9 ± 42.5 μm which is also shorter compared to the SS316L-CoNi joint. Beyond the grain coarsening boundary, the average size of the SS316L fine grains is 14.67 ± 10.79 μm, this is smaller than the size displayed by the SS316L-CoNi joint. There was no significant change in the grain size of the CoCrNi alloy after the welding process.

For the SS316L-CoCrFeNi joint (Fig. 8(g – h)), the bond was almost defect-free with even fewer interfacial pores of the average size of 0.4 ± 0.1 μm only noticeable at high magnification. A few microvoids were also noticed randomly scattered within the microstructure. SS316L grain coarsening was observed near the bond interface covering a width of 337.4 ± 36.5 μm from the bond interface to the grain coarsening boundary. The average size of coarse SS316L grains is about 40 ± 8.2 μm which is smaller in comparison to the CoNi and CoCrNi joints. The average size of the SS316L fine grains beyond the grain coarsening boundary is 14.86 ± 11.57 μm and this is similar to the size observed with the SS316L-CoCrNi joint. The grain size within the CoCrFeNi alloy remained almost the same even after welding.

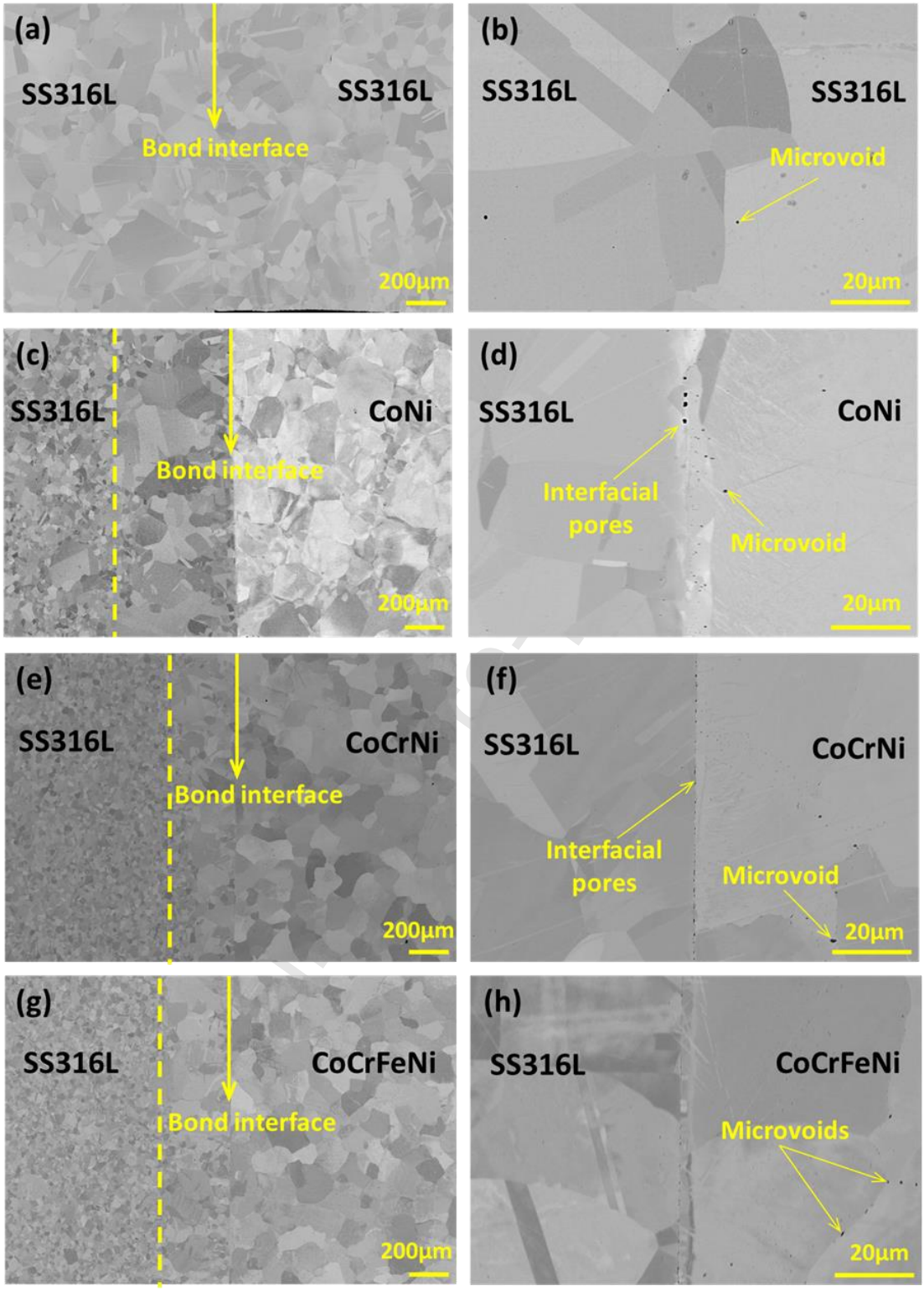

Fig. 8. SEM micrographs at low and high magnifications of the SS316L diffusion welded joints with, (a – b) SS316L, (c – d) CoNi, (e – f) CoCrNi, and (g – h) CoCrFeNi. Yellow dashed lines indicate the end of the grain coarsening zone. In Fig. 8(a), the grain coarsening zone is the entire SS316L microstructure.

Table 2. Summary of quantitative parameters measured using ImageJ within the microstructure of the diffusion-welded samples

Joints	Width of SS316L grain coarsening zone (μm)	Average size of SS316L coarse grains (μm)	Average size of SS316L fine grains (μm)	Grain size of MCAs (μm)	Average size of interfacial pores (μm)
SS316L-SS316L	Whole	78.6 ± 16.5	N/A	N/A	Nil
SS316L-CoNi	645.6 ± 43.0	77.4 ± 15.2	20.6 ± 13.6	106.7 ± 18.3	0.9 ± 0.2
SS316L-CoCrNi	256.9 ± 42.5	49.7 ± 11.9	14.7 ± 10.8	90.2 ± 14.4	0.4 ± 0.2
SS316L-CoCrFeNi	337.4 ± 36.5	40.0 ± 8.2	14.9 ± 11.6	84.0 ± 10.1	0.4 ± 0.1

3.2.2 EBSD microstructural examination of the welded joints

Further examination of the diffusion welded joint microstructures was conducted based on the EBSD orientation maps presented in Fig. 9. The SS316L similar joint (Fig. 9(a)) displayed homogeneous grain growth throughout the entire microstructure with evidence of annealing twins. Almost 99% of the grains presented high angle grain boundary (HAGB) while only about 1% showed low angle grain boundary (LAGB). The maps in Fig. 9 (b – d) revealed that there was heterogeneous grain growth within the SS316L microstructures with several coarse grains mainly concentrated near the bond interface. Few coarse grains are also found randomly scattered within the SS316L microstructure indicating abnormal grain growth. Several fine grains also co-exist with these coarse grains near the bond interface but the fine grains prominently dominate the microstructure far away from the interface after the grain coarsening zone. The SS316L grains presented annealing twins for all the joints while only the CoNi grains revealed annealing twins near the bond interface but no twin was found at the region far from the bond interface. The CoCrNi and CoCrFeNi grains do not present any annealing twins in their microstructures. Nearly 98% of the grains have HAGB with the LAGB

accounting for only about 2%. A high fraction of HAGB is associated with recrystallization. Although new grains are formed across the entire microstructure, the recrystallization that occurred in SS316L is non-uniform and could also be termed inhomogeneous recrystallization. The EBSD analysis of the four joints only revealed a single face-centred cubic (FCC) phase throughout the entire microstructure. No secondary or detrimental intermetallic phase was observed at the bond interface or around the diffusion zone.

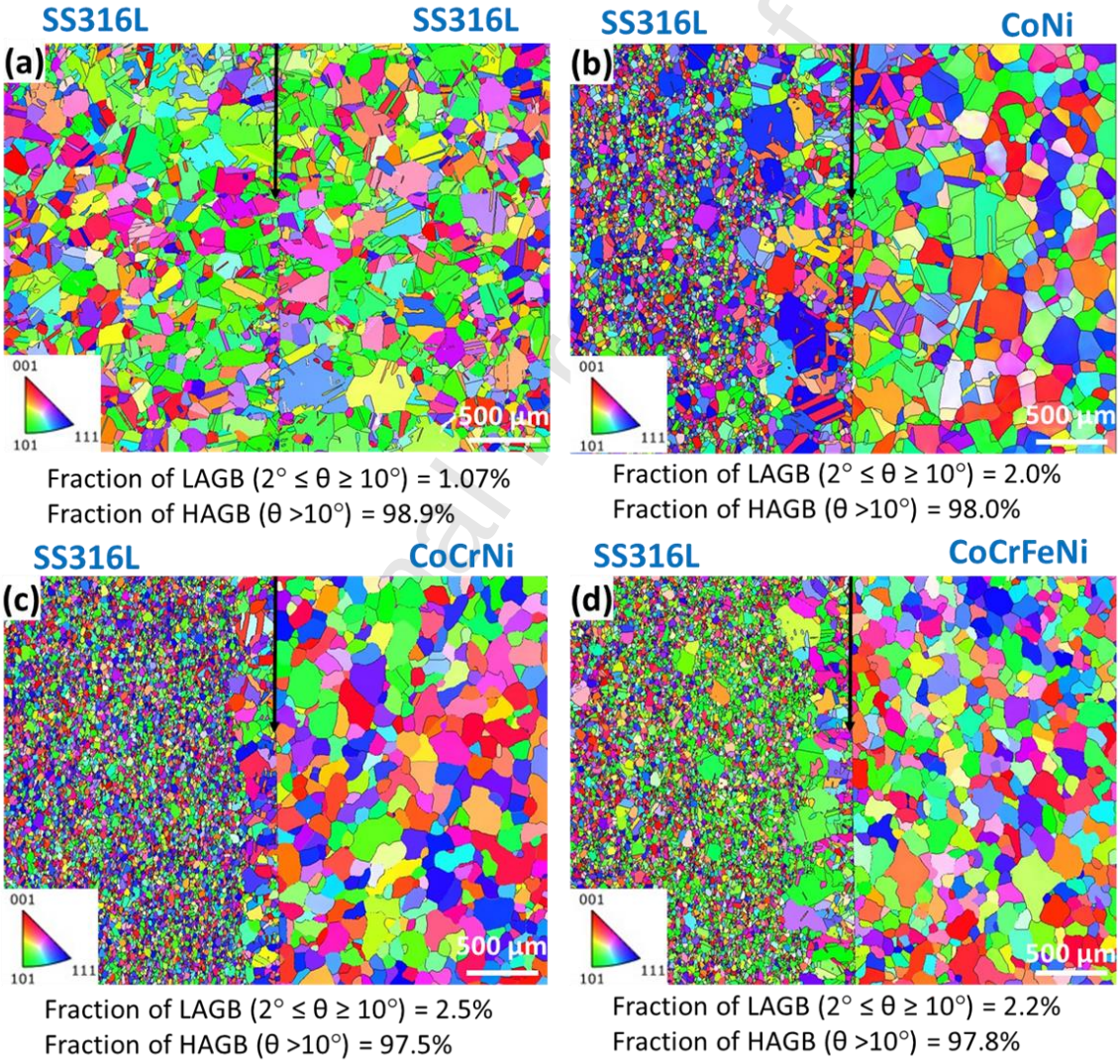

Fig. 9. Low magnification EBSD orientation maps with the inverse pole figures (IPF) as inset providing an overview of the grain variation within the microstructure of (a) SS316L-SS316L joint (b) SS316L-CoNi joint (c) SS316L-CoCrNi joint (d) SS316L-CoCrFeNi joint.

3.3 Chemical composition analyses of the welded samples by SEM-EDS

3.3.1 Elemental distribution across the bond interfaces

The line profiles of the elemental composition across the bond interface for the three MCAs are represented in Fig. 10. The concentration of the diffusing elements in the welded samples is presented with respect to the positions from the interfaces. The major constituents of SS316L are Fe, Cr and Ni having initial atomic concentrations of about 70%, 18% and 9% respectively, while all the MCAs (CoNi, CoCrNi and CoCrFeNi) contained elemental composition in equiatomic ratios. An interdiffusion zone was created which is the mixing area of diffused atoms from both SS316L and the MCAs and can be delimited by the bond interface visible on the SEM images. Using the bond interface as the reference point, the diffusion zone is divided into two zones representing the SS316L side (zone I) and the MCA side (zone II). The diffusion widths at zone I and II were determined based on the interval between the bond interface and the points where the elements attain compositional stability on the chemical line scan data at the SS316L and MCA side respectively. Since the diffusion widths at zone I and II for all the elements are different, the highest diffusion width observed at both sides was taken and the addition of the two values gave the global diffusion width for each joint.

For the SS316L- CoNi assembly (Fig. 10(a)), Fe and Cr atoms diffused away from SS316L steadily across the bond interface towards the CoNi binary alloy hence the concentration of these elements also gradually diminishes as we move closer to the bond interface at the SS316L side. On the CoNi alloy side, due to the high concentration of Co and Ni atoms, they diffused towards the SS316L base metal and their concentration also decreased as we approached the bond interface. At the SS316L side, Ni-enrichment could be detected near the

bond interface. The entire diffusion width is 29.9 µm with zone I and zone II having widths of 10.1 µm and 19.8 µm respectively. The width of Zone II is greater than that of Zone I. In the case of SS316-CoCrNi assembly (Fig. 10(b)), Co, Ni and Cr atoms diffused away from the CoCrNi alloy side across the bond interface towards the SS316L while only the Fe atom diffused from SS316L away towards the CoCrNi alloy side. The total diffusion width across the bond interface was 14.3 µm with width at zone I being 3.6 µm and that of zone II was 10.7 µm. Elemental diffusion was also higher in Zone II than in Zone I. The diffusion trend observed in the SS316L-CoCrFeNi assembly (Fig. 10(c)) is similar to that of the SS316L-CoCrNi joint as only Fe atom diffused towards the CoCrFeNi alloy while Co, Ni and Cr atoms diffused towards the side of SS316L. The entire diffusion width is 13.6 µm, where the diffusion width at zone I is 7.8 µm and zone II is 5.8 µm.

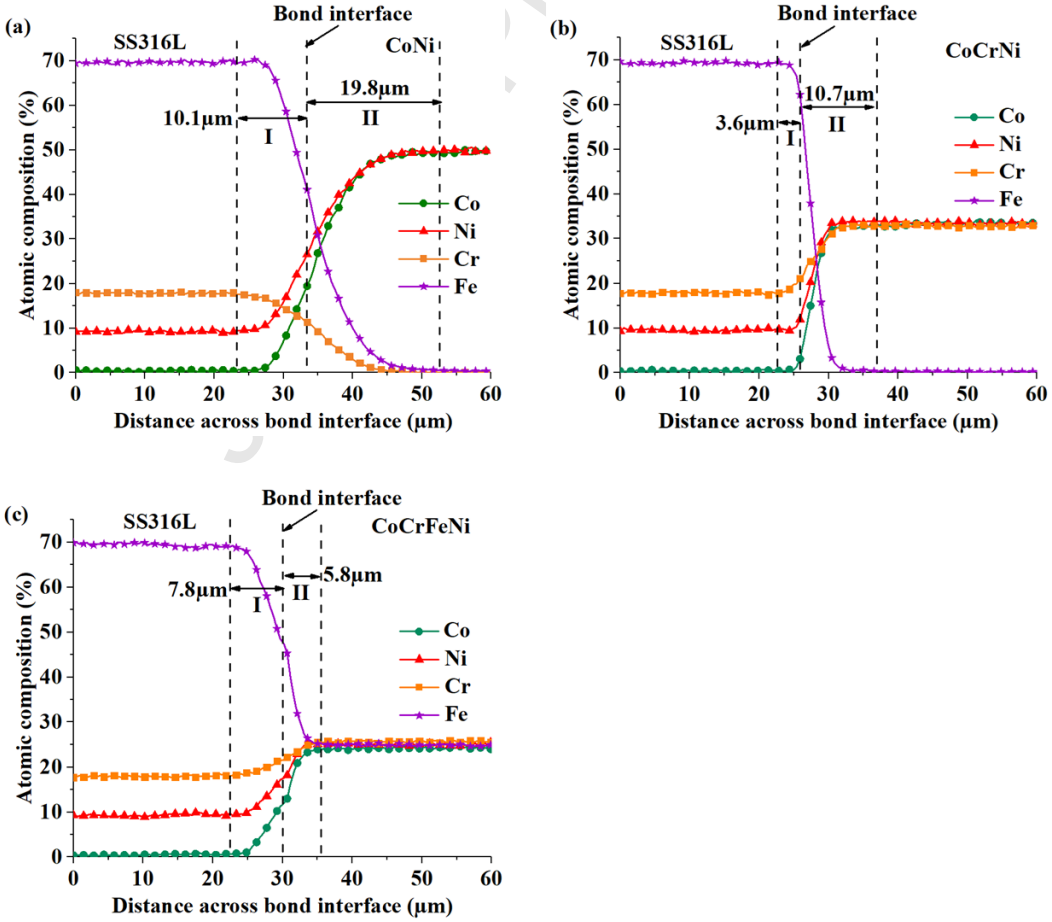

Figure 10. Chemical gradients across the bond interfaces as determined by EDS analyses for, (a) SS316L-CoNi joint, (b) SS316L-CoCrNi joint, (c) SS316L-CoCrFeNi joint

3.3.2 Diffusion coefficients of major elements in the joints

The diffusion behaviour of atoms at the bond interfaces can be better understood by evaluating the diffusion coefficients of the major elements that enriched the interfaces. The diffusion coefficient, *D*, was analytically determined based on Fick's second law of diffusion. For semi-infinite length diffusion, the one-dimensional relationship between elemental concentration, *C*, and distance from the interface, *x*, can be expressed as:

$$\frac{\partial C}{\partial t} = D\frac{\partial^2 C}{\partial x^2} \quad \text{(Eq. 1)}$$

To solve Eq. 1, a numerical integration scheme based on the finite difference method was adopted by discretizing the space and time with regular increments, Δx and Δt, respectively. Thus, the expression of the concentration of the element *(i)*, $C_{(i)}$, at the position x and time t can be given as follows:

$$C_{(i)}(x, t) = C_{(i)}(x, t-\Delta t) + D\,[C_{(i)}(x+\Delta x, t-\Delta t) + C_{(i)}(x-\Delta x, t-\Delta t) - 2\,C_{(i)}(x, t-\Delta t)]\,\Delta t/\Delta x^2. \quad \text{(Eq. 2)}$$

The value of the diffusion coefficient, *D,* is different according to the position, x, in SS316L and MCA. At the interface (x = 0), the diffusion coefficient is the average value of the two diffusion coefficients. The boundary conditions are:

$$\text{At } t = 0: C = C_0 \text{ (SS316L) for } x < 0 \text{ and } C = C_o \text{ (MCA) for } x > 0 \quad \text{(Eq. 3)}$$

$$\text{At } t > 0: C = C_o \text{ (SS316) for } x < 40\ \mu m \text{ and } C = C_o \text{ (MCA) for } x > 40\ \mu m$$

The diffusion is assumed to be negligible during heating and cooling, so the diffusion coefficient is assumed to be constant during the whole diffusion time of 1 hour at 1075°C. Distance step Δx is 1 µm and time step, Δt is 4 s. The chemical composition line distribution in Fig. 10 provided information on the elemental concentration and distance from the bond interface which was used to calculate the diffusion coefficient by Eq. 2.

Table 3 shows the values of the diffusion coefficients at zones I and II under a welding temperature of 1075°C for an exposure time of 1 hour. From the results, the sequence of diffusion of elements across the bond interfaces in order of decreasing diffusion coefficients for both the SS316L-CoNi and SS316L-CoCrNi joints is Cr > Fe > Ni > Co while for the SS316L-CoCrFeNi joint, the sequence is Cr > Ni > Co > Fe. A higher diffusion coefficient implies a faster diffusion rate and an easier elemental mass transport.

Table 3. Diffusion coefficients, D of major elements at zone I (SS316L side) and zone II (MCA side) under a bonding temperature of 1075°C for 1 hour (Diffusion coefficients of atoms moving across the bond interface into new materials are highlighted). The error bar is about ±10%.

Joints	Diffusion coefficients (x 10^{-15} m^2/s)	D_{Co}	D_{Ni}	D_{Cr}	D_{Fe}
SS316L-CoNi	Diffusion at Zone I	**1.40**	**2.00**	3.20	1.60
	Diffusion at Zone II	3.60	5.00	**4.30**	**4.25**
SS316L-CoCrNi	Diffusion at Zone I	**0.15**	**0.20**	**0.90**	0.20
	Diffusion at Zone II	0.40	0.35	0.50	**0.45**
SS316L-CoCrFeNi	Diffusion at Zone I	**1.50**	**1.70**	**2.00**	1.50
	Diffusion at Zone II	0.50	0.50	1.10	**0.50**

3.3.3 Grain size variation within the diffusion zone

It is well known that in polycrystalline materials, grain boundaries are major diffusion channels hence, it is important to further investigate the grain size distribution within the diffusion zones (zone I and zone II). Table 2 provides a summary of the grain distribution within the microstructure of MCAs in the welded samples. The sequence of grain size at diffusion zone II (MCAs side) in order of decreasing grain size is CoNi > CoCrNi > CoCrFeNi. Due to the heterogeneous grain growth observed in SS316L, zoom EBSD orientation maps of the three welded joints were taken and presented in Fig. 11. It was revealed that fine and

coarse grains co-existed near and within the diffusion zone I (SS316L side). Quantitative assessment of the SS316L grains within the diffusion zone as reported by the AZtecCrystal software is presented in Table 4. The grain sizes in these joints range from 6.1 to 43.2 µm for the joint with binary alloy, from 7.9 to 57.9 µm for the joint with ternary alloy and from 5.4 to 56.6 µm for the joint with quaternary alloy. The average size of SS316L grains within the diffusion zone for SS316L-CoNi, SS316L-CoCrNi and SS316L-CoCrFeNi joints are 20.5 ± 10.9 µm, 21 ± 10.9 µm and 20.3 ± 16.6 µm respectively. This implies that the fraction of fine grains within the diffusion zone is more than that of coarse grains. Consequently, variation in the diffusion coefficients of the elements at zone I for the three joints is not majorly a function of the grain boundaries since there is no wide variation in the average size of SS316L grains within the diffusion zone for the three joints. Fig. 11 also reveals several annealing twins in all the welded samples at the SS316L side, the CoNi alloy microstructure also shows some twins.

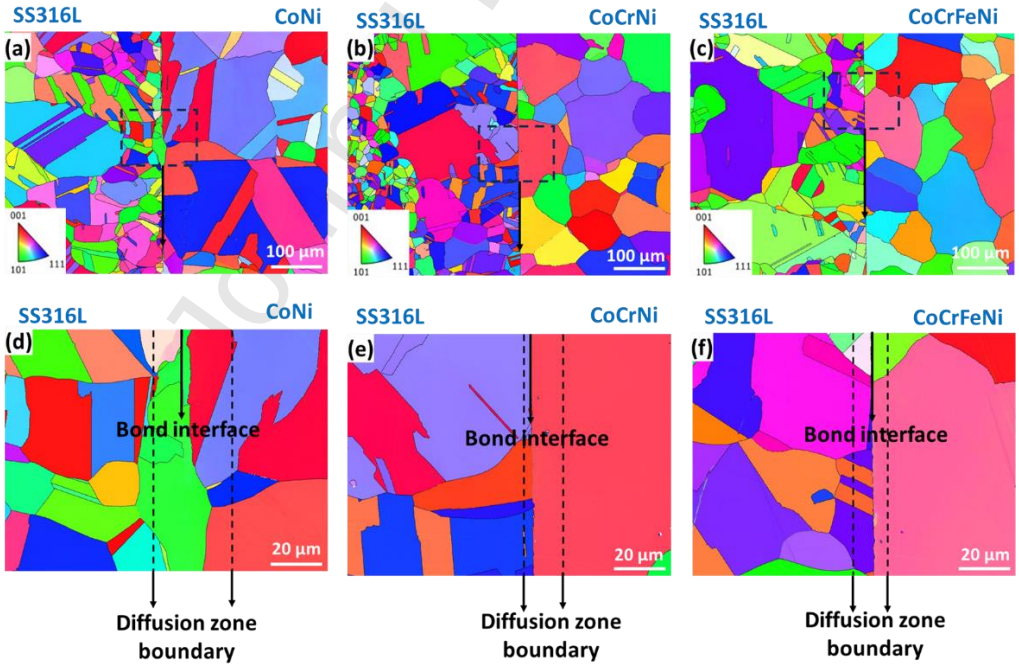

Fig. 11. EBSD orientation maps at different magnifications showing the grain size variation within the diffusion zone (a,d) SS316L-CoNi joint, (b,e) SS316L-CoCrNi joint, (c,f) SS316L-CoCrFeNi joint.

Table 4. Summary of the sizes of SS316L grains within the diffusion zone of the welded joints

Joints	Minimum grain size (µm)	Maximum grain size (µm)	Average grain size (µm)
SS316L-CoNi	6.1	43.2	20.5 ± 10.9
SS316L-CoCrNi	7.9	57.9	21.0 ± 10.9
SS316L-CoCrFeNi	5.4	56.6	20.3 ± 16.6

3.4 Shear properties of welded samples

The mechanical responses in terms of the shear strength and shear strain to rupture of all the diffusion welded joints were assessed based on the shear test results presented in Fig. 12. The SS316L-CoNi joint had the lowest shear strength of 251 MPa, while the SS316L-CoCrFeNi joint had the highest shear strength of 402 MPa, SS316L-CoCrNi joint had a shear strength of 311 MPa. The shear strength of a similar joint of SS316L is 383 MPa. The shear strain to rupture of the joints which is an indication of the ductility of the joints is also presented. SS316L-CoNi joint displayed the lowest ductility of 10.3% while SS316L-CoCrNi and SS316L-CoCrFeNi joints had better ductility of 15.2% and 14.8% respectively which is closer to the ductility of SS316L similar joint of 19.7%. SS316L-CoCrNi and SS316L-CoCrFeNi joints had good mechanical responses with their shear strength and ductility close to that of SS316L similar joints.

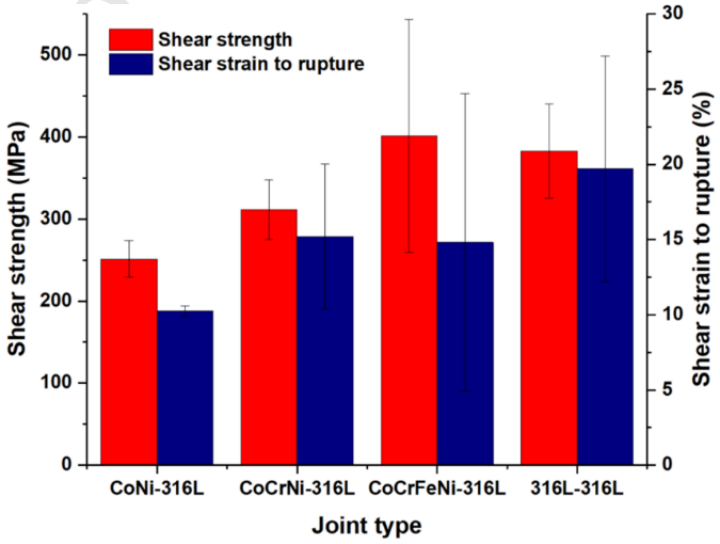

Fig. 12. Shear test results for the diffusion welded joints show the shear strength and shear strain to rupture.

3.5. Fractography of the ruptured surfaces

To understand the mode of fracture and to determine the location where it occurs, the fractographs of the samples obtained after the shear test were critically examined. The micrographs shown in Fig. 13 reveal the surface morphologies of the fractured samples. The fracture surfaces shown in Fig. 13 (a, c & e) are those of SS316L for all three joints while Fig. 13 (b, d & f) are for the MCAs. The fractured surfaces presented in Fig. 13(a – b) are for the SS316L-CoNi joint which is characterised by fine shallow dimples. The presence of dimples implies ductile fracture mode. Fig. 13 (c – d) presents the surface topography of the ruptured SS316L-CoCrNi joint which is characterised by coarse dimples. Cavities are also found which are formed by the growth and coalescence of voids due to plastic deformation. All these features are confirmation of a ductile fracture in the joint. The fractographs of the SS316L-CoCrFeNi joint shown in Fig. 13 (e – f) also revealed ductile fracture with features similar to those noticed in the SS316L-CoCrNi joint. The coarse dimples revealed in these two joints implies they have superior ductility to that of SS316L-CoNi joint. The CoCrFeNi part was subjected to severe plastic deformation before failure which led to a pronounced shear lip that was observed in a macroscopic view (not shown in the figures). The EDS chemical analyses of some locations on the fractographs were taken to determine where the fracture occurred and the results are presented in Table 5. The marks P1 and P2 are on the SS316L-CoNi fractured surfaces, the chemical composition of these points corresponds to the area within the diffusion zone at the CoNi alloy side. From these results, for the SS316L-CoNi joint, the fracture occurred at zone II (CoNi side). P3 and P4 are on the SS316L-CoCrNi ruptured

surfaces and the chemical composition of these points revealed that the fracture occurred at zone I closer to the bond interface. The points P5 and P6 are on the SS316L-CoCrFeNi fractured surfaces, the chemical composition of P5 corresponds to a point at zone I (SS316L side) while P6 only reveal the composition of the parent alloy. Hence, it can be inferred that the fracture of the SS316L-CoCrFeNi joint occurred at zone I which is on the SS316L side.

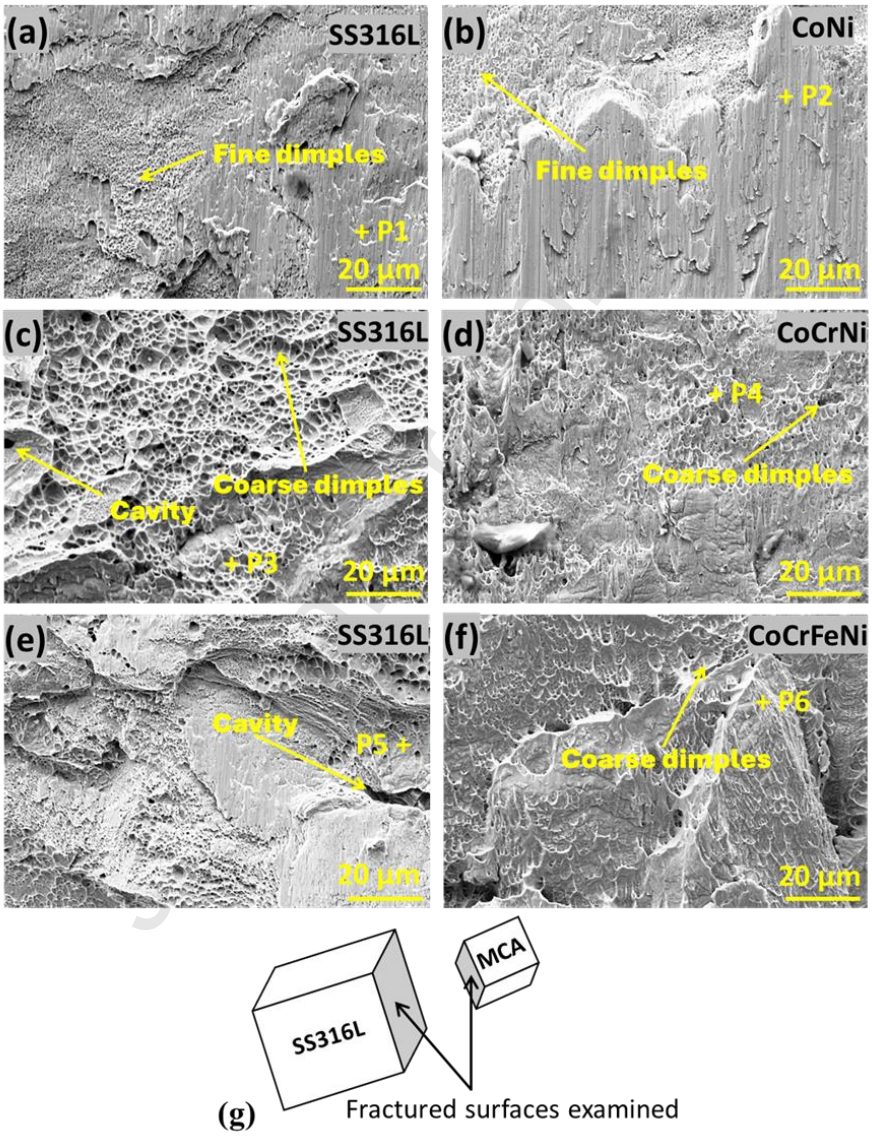

Fig. 13. Microstructures of the fractured samples showing various features, (a – b) SS316L-CoNi diffusion welded sample, (c - d) SS316L-CoCrNi DFW sample, (e - f) SS316L-CoCrFeNi DFW sample (g) SS316L and MCA fractured surfaces examined.

Table 5. Chemical composition (at. %) at the marked locations in Figure 13 (Zone I is at SS316L side and Zone II is at MCA side)

Joint	Pos.	Co	Ni	Cr	Fe	Mn	Fracture location
SS316L-CoNi	P1	24.85	31.34	10.03	31.47	0.77	Zone II
	P2	25.89	31.00	9.71	30.82	0.69	Zone II
SS316L-CoCrNi	P3	4.41	12.54	22.64	57.86	1.35	Zone I closer to interface
	P4	4.20	12.57	23.50	57.47	1.13	Zone I closer to interface
SS316L-CoCrFeNi	P5	7.86	13.30	22.51	54.00	1.10	Zone I
	P6	25.20	24.82	26.40	23.00	0.03	CoCrFeNi

3.6 Phase analyses of the fractured surfaces

The result of the XRD phase analyses of all the fractured samples is presented in Fig. 14. The diffraction patterns in Fig. 14(a) are those of the SS316L surfaces while Fig. 14(b) are the patterns for the MCAs. All the patterns display peaks at {111}, {200} and {220} which are similar to those observed in the parent samples in Fig. 7 and these are characteristics of FCC crystals. However, the XRD patterns of the fractured SS316L-CoCrNi and SS316L-CoCrFeNi joints reveal additional small peaks at 2θ ~ 52° and 2θ ~ 78° from the {110} and {200} planes respectively which could be coming from martensite induced during fracture. It is important to also note that no carbide-based intermetallic peaks were observed.

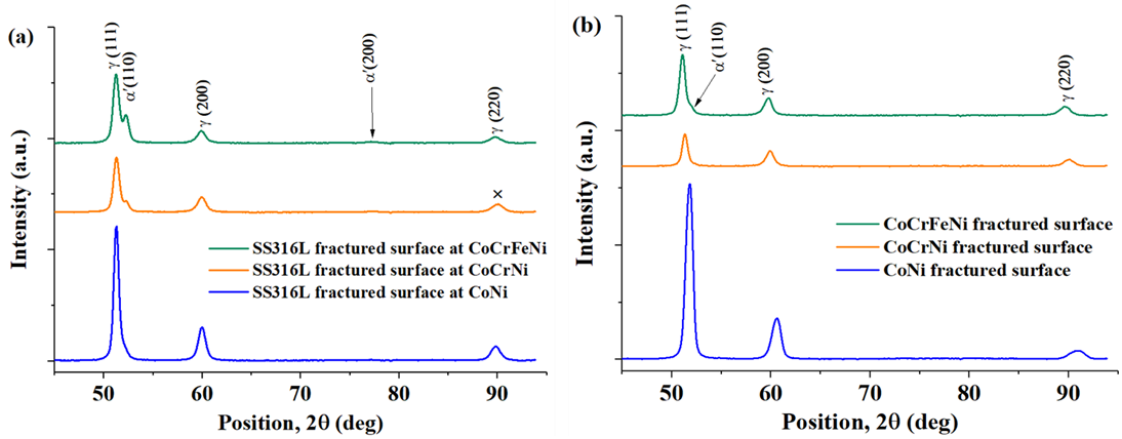

Fig. 14. XRD patterns of the three welded fractured surfaces, (a) SS316L surfaces (b) MCAs surfaces.

4. Discussion

The three MCAs selected for this work were successfully joined to SS316L with minimal interfacial defects and microvoids. By comparing the dissimilar welding of SS316L-MCA with that of similar welding of SS316L, it was observed that the SS316L similar welding had better material continuity as the bond interface was less visible and there was microstructural growth across the interface of the joint. Diffusion welding of two samples takes place in three stages [21]. The first stage involves heat and pressure application resulting in the deformation of the grains at the interface of the workpieces, the grain boundaries are still defined and there are still voids between the interface. In the second stage, diffusion becomes more prevalent as atoms migrate to new positions and pores from the valleys disappear. The third stage leads to volume diffusion of atoms, boundary disappearance, formation of new grains across the interface and pores elimination. Since it is impossible to achieve 100% tight contact with the welding surfaces, a few isolated pores may still exist at this stage but they are likely to have little influence on the joint integrity.

The diffusion zones formed around the bond interfaces for all the joints due to the interdiffusion of elements across the base materials consist of a single FCC phase intermetallic. The chemical composition profiles in Fig. 10, the back-scattered electron (BSE) images at high magnification, and EBSD analyses of the joints as well as the EDS and XRD analyses of the fractured welded samples did not reveal any compositional segregation, multiple phases or intermetallic carbides. Spark plasma-assisted diffusion bonding of 316L with equiatomic CoCrNi, CoCrFeNi, and CoCrFeMnNi was conducted by Sun et al. [32] at a temperature of 1050°C, and bonding pressure of 25MPa for 1hr. A continuous FCC solid solution structure was formed in the diffusion zone. Another study conducted by Samiuddin et al. [30], [31] examined diffusion welding of 304 stainless steel and equiatomic CoCrNi at

welding temperatures of 1050°C and 1075°C, bonding pressure of 5 MPa and bonding time of 1 hr. These studies also concluded that FCC solid solution structure was formed at the bond interfaces although, this phase was accompanied by some carbide-based intermetallic phases majorly chromium carbide. This was reported to be due to the higher carbon content of 304 stainless steel. However, the SS316L used in this study has a carbon content of about 0.02 wt% hence, its low carbon content may have prevented the formation of intermetallic carbides within the diffusion zone.

Table 3 shows that the joint with the binary alloy had relatively higher elemental diffusion coefficients compared to the other joints and this is an indication of a faster diffusion rate. The high diffusion coefficients in this joint can be attributed to the fact that CoNi alloy contains only two elements hence, the crystal structure is less distorted. Low lattice distortion is indicative of low configurational entropy hence, diffusion across such material will be easier and faster due to possible lower activation energy in this case [38]. This provides the basis for the SS316L-CoNi joint to have the largest diffusion width at zones I and II (Diffusion width at zone I < Diffusion width at zone II) when compared to other joints as observed in Fig. 10(a). The sequence of the diffusion coefficients in decreasing order for SS316L-CoCrNi joint is similar to that of SS316L-CoNi joint (Cr > Fe > Ni > Co) but the values of the diffusion coefficient in this case are lower. This can be attributed to an additional element in the ternary alloy which will cause more lattice distortion and lead to higher configurational entropy within the crystal structure hence, making the diffusion process in this case more difficult [38], [39]. For the SS316L-CoCrFeNi joint, there is a difference in the sequence of the diffusion coefficients compared to the other joints (Cr > Ni > Co > Fe). The values of diffusion coefficients are also lower than those observed in the joint with binary alloy but higher than that of the joint with

ternary alloy, especially at zone I. As the Cr composition of SS316L and CoCrFeNi are very close, the diffusion coefficient may have been calculated with a high error for this element. The smaller size of CoCrFeNi grains compared to that of CoCrNi grains (Table 2) may have been responsible for the higher diffusion coefficients of Co, Ni and Cr atoms at zone I in SS316L-CoCrFeNi joint. It has been reported that fine grains with several grain boundaries will provide more channels for atomic diffusion than large grains [40]. The higher diffusion coefficients displayed by these atoms in zone I for the quaternary joint translated to the longer diffusion width of about 8 µm. At zone II, the diffusion width of about 6 µm observed for the SS316L-CoCrFeNi joint was smaller than that of the SS316L-CoCrNi joint which was about 11µm. This can be attributed to the higher configurational entropy because of the presence of more elements in the quaternary alloy as compared to the ternary alloy. The diffusion mechanism observed in the ternary and quaternary joints is similar in terms of elements that diffused across the bond interface but the overall diffusion widths (zone I and II) of these two joints are 14.3 µm and 13.6 µm for the ternary and quaternary joints respectively. This is a departure from the large diffusion width of 29.9 µm displayed for the binary joint. The joint between 304 stainless steel and equiatomic CoCrNi earlier reported [30], [31], displayed overall diffusion widths of 10 µm and 19 µm at welding temperatures of 1050°C and 1075°C respectively. It was reported that the Fe atom was mainly responsible for the development of bond interface due to its high diffusive character. The sequence of the diffusion coefficients of the elements in decreasing order is Fe > Cr > Ni > Co. The diffusion coefficients of Cr diminished due to chromium interaction with carbon to form Cr-based carbide. For this study, due to the low composition of carbon in SS316L, the Cr atom had the highest diffusivity. Hence, an overall diffusion width of 14 µm was obtained when the SS316L-CoCrNi joint was produced by conventional diffusion welding aligned with previous works. It

is important to note that the diffusion coefficient strongly depends on several factors which include the material composition, crystal structure, degree of lattice distortion or configurational entropy, crystal orientation, dislocation densities, vacancies, grain boundaries due to grain sizes within the microstructure [41]. Therefore, one single factor is not responsible for the rate of diffusion of atoms in the joints but a combination of these factors. Good understanding of how these factors interact and control diffusion is imperative.

Thermal exposure of SS316L between 955 – 1120°C will fully softens the steel [42]. Hence, the mechanical responses of the base alloys must have been altered due to the coarsening of the SS316L grains. Larger grains in SS316L have been reported to have much wider chromium-depleted zones and lower grain boundary chromium concentrations in diffusion bonded SS316L joint [43]. Hence, these characteristics could improve the resistance of the joints to intergranular corrosion. It is a challenge in diffusion welding involving SS316L to obtain optimized grain size without sometimes compromising the mechanical properties of the material. Although the SS316L-CoNi joint had the largest diffusion width compared to other joints, it did not translate into a mechanically superior joint. SS316L-CoCrNi and SS316L-CoCrFeNi assemblies presented good mechanical responses (shear strength and ductility) comparable to that of SS316L similar joints. The overall diffusion widths of these two joints are within close range. The microstructures of the diffusion welded samples revealed that the SS316L-CoNi joint had the largest interfacial pores and MCA grain size, the SS316L softened zone is also the widest compared to the two other joints. It is well known that smaller grains have a higher resistance to fracture because a crack in such material has more difficulty moving across several small grains than across larger ones. In addition, the fractured surfaces of the SS316L-CoNi joint was dominated by fine dimples while the two other joints displayed

coarser dimples which is an evidence of higher ductility and perhaps superior mechanical response compared to the joint with the binary alloy. Equiatomic CoCrNi has been reported to display exceptional strength-toughness properties and damage tolerance [6]. There are also reports that dissimilar welding of stainless steel to equiatomic CoCrNi joint had an excellent combination of strength and ductility that exceeds those of other dissimilar HEA joints and most similar HEA joints at room and cryogenic temperatures [15], [30]. CoCrFeNi alloy is the most compatible with SS316L in terms of chemical composition compared to the binary and ternary alloys, this may have contributed to the good mechanical responses that were observed when SS316L was diffusion welded with the quaternary alloys.

For the joint between 304 stainless steel and CoCrNi [30], [31], the shear strength obtained was 505 MPa and 498 MPa when diffusion welding was carried out at 1075°C and 1050° C respectively. The SS316L-CoCrNi and SS316L-CoCrFeNi joints examined by Sun et al. [32] displayed tensile strengths of about 580MPa and 460MPa respectively, both values are more than 80% of the tensile strength of SS316L base metal. For this study, the shear strengths of SS316L-CoCrNi and SS316L-CoCrFeNi joints were 311 MPa and 402 MPa respectively and both joints are also above 80% of the shear strength of SS316L similar joints. In comparing the mechanical properties of different studies, it is important to note that the stress distribution at the bond interfaces during shear tests may be very heterogeneous. The results obtained may differ due to specimen dimensions, surface geometry, composition, specimen preparation and loading conditions. Failure usually occurs due to stress concentration around defects or voids at the interface which causes a crack to propagate.

5. Conclusions

A comprehensive experimental study was successfully carried out to investigate diffusion welding of equiatomic CoNi, CoCrNi and CoCrFeNi alloys to 316L stainless steel. The microstructural evolution and diffusion mechanism of each joint were examined using a Scanning Electron Microscope (SEM) equipped with an Energy Dispersive Spectrometer (EDS), Electron Back Scattered Diffraction (EBSD) and X-ray Diffraction (XRD) analyses. The diffusion coefficients of the major elements were determined based on Fick's second law of diffusion. The mechanical responses of all the joints were assessed by a shear test, and the XRD patterns of the diffusion welded fractured samples were finally investigated. The following findings are made:

i) The equiatomic CoNi, CoCrNi and CoCrFeNi alloys were all successfully joined to SS316L with minor interfacial defects which did not significantly influence the joint integrity.

ii) Diffusion zones consisting of a single FCC phase were formed across the bond interfaces due to the interdiffusion of constitutive elements and their widths are dependent on the diffusion coefficients of these elements. No compositional segregation or secondary intermetallic phases were noticed.

iii) The chemical complexity of the alloys welded to SS316L significantly influenced the diffusion coefficients of constituent elements among other important factors.

iv) SS316L-CoCrNi and SS316L-CoCrFeNi joints offered good shear strength of 311 MPa and 402 MPa, respectively, and ductility of 15.2% and 14.8%, respectively, these two dissimilar joints having comparable properties to the SS316L similar joint. The SS316L-CoNi joint had the least shear strength and ductility.

The effect of the thermal exposure in terms of welding temperature and time should be investigated to optimise the diffusion welding process. The influence of oxidation and

corrosion on the integrity of dissimilar diffusion welded joints should also be issues of concern.

Declaration of competing interests

The authors declare that they have no known competing financial interests or personal relationships that could have appeared to influence the work reported in this paper.

Acknowledgements

This research was financially supported by the Petroleum Technology Development Fund (PTDF), Nigeria. The authors acknowledge the experimental facilities (MicroMat) from LEM3 (Université de Lorraine - CNRS UMR 7239). The authors would also like to appreciate Auriane Mandrelli, Yudong Zhang, Olivier Perroud of the LEM3 laboratory and Marc Wary (Ecole Nationale Superieure Arts et Metiers) for their technical support.

References

[1] M. John *et al.*, 'Welding Techniques for High Entropy Alloys: Processes, Properties, Characterization, and Challenges', *Materials*, vol. 15, no. 6, p. 2273, Mar. 2022, doi: 10.3390/ma15062273.
[2] J. G. Lopes and J. P. Oliveira, 'A Short Review on Welding and Joining of High Entropy Alloys', *Metals*, vol. 10, no. 2, p. 212, Feb. 2020, doi: 10.3390/met10020212.
[3] B. S. Murty, J. W. Yeh, S. Ranganathan, and P. P. Bhattacharjee, *High-entropy alloys*, Second edition. Amsterdam, Netherlands ; Cambridge, MA: Elsevier, 2019.
[4] J.-W. Yeh, 'Recent progress in high-entropy alloys', *Ann. Chim. Sci. Mat.*, vol. 31, no. 6, pp. 633–648, Dec. 2006, doi: 10.3166/acsm.31.633-648.
[5] C. D. Gómez-Esparza *et al.*, 'Comparison of Microstructure and Hardness of an Equiatomic NiCo Alloy Produced by Two Routes.', *Microsc Microanal*, vol. 22, no. S3, pp. 1994–1995, Jul. 2016, doi: 10.1017/S1431927616010813.
[6] B. Gludovatz *et al.*, 'Exceptional damage-tolerance of a medium-entropy alloy CrCoNi at cryogenic temperatures', *Nat Commun*, vol. 7, no. 1, p. 10602, Feb. 2016, doi: 10.1038/ncomms10602.
[7] M. Shabani, J. Indeck, K. Hazeli, P. D. Jablonski, and G. J. Pataky, 'Effect of Strain Rate on the Tensile Behavior of CoCrFeNi and CoCrFeMnNi High-Entropy Alloys', *J. of Materi Eng*

and Perform, vol. 28, no. 7, pp. 4348–4356, Jul. 2019, doi: 10.1007/s11665-019-04176-y.

[8] D. Afonso *et al.*, 'Dissimilar laser welding of an as-rolled CoCrFeMnNi high entropy alloy to Inconel 718 superalloy', *Optics & Laser Technology*, vol. 180, p. 111427, Jan. 2025, doi: 10.1016/j.optlastec.2024.111427.

[9] J. Shen *et al.*, 'Synergistic effects of Monel 400 filler wire in gas metal arc welding of CoCrFeMnNi high entropy alloy', *Materials & Design*, vol. 242, p. 112996, Jun. 2024, doi: 10.1016/j.matdes.2024.112996.

[10] J. R. Davis, Ed., *Stainless steels*. in ASM specialty handbook. Materials Park, Ohio: ASM International, 1994.

[11] Q. Lu *et al.*, 'Reveal the Viscoplastic Behaviour and Microstructure Evolution of Stainless Steel 316L', *Materials*, vol. 15, no. 20, p. 7064, Oct. 2022, doi: 10.3390/ma15207064.

[12] B. Gludovatz, A. Hohenwarter, D. Catoor, E. H. Chang, E. P. George, and R. O. Ritchie, 'A fracture-resistant high-entropy alloy for cryogenic applications', *Science*, vol. 345, no. 6201, pp. 1153–1158, Sep. 2014, doi: 10.1126/science.1254581.

[13] ASM International, Ed., *Metals handbook: irons, steels, and high-performance alloys*, 10th ed. Materials park (Ohio): ASM international, 1990.

[14] T. S. Srivatsan and M. Gupta, Eds., *High entropy alloys: innovations, advances, and applications*. Boca Raton: CRC Press, 2020.

[15] S. Yan, H. Zhou, Z. Zhu, Y. Fu, and J. Tian, 'High strength-ductility synergy in a laser welded dissimilar joint of CrCoNi medium-entropy alloy and stainless steel', *Materials Science and Engineering: A*, vol. 840, p. 142854, Apr. 2022, doi: 10.1016/j.msea.2022.142854.

[16] J. P. Oliveira *et al.*, 'Dissimilar laser welding of a CoCrFeMnNi high entropy alloy to 316 stainless steel', *Scripta Materialia*, vol. 206, p. 114219, Jan. 2022, doi: 10.1016/j.scriptamat.2021.114219.

[17] R. Sokkalingam, V. Muthupandi, K. Sivaprasad, and K. G. Prashanth, 'Dissimilar welding of Al $_{0.1}$ CoCrFeNi high-entropy alloy and AISI304 stainless steel', *J. Mater. Res.*, vol. 34, no. 15, pp. 2683–2694, Aug. 2019, doi: 10.1557/jmr.2019.186.

[18] N. K. Adomako, G. Shin, N. Park, K. Park, and J. H. Kim, 'Laser dissimilar welding of CoCrFeMnNi-high entropy alloy and duplex stainless steel', *Journal of Materials Science & Technology*, vol. 85, pp. 95–105, Sep. 2021, doi: 10.1016/j.jmst.2021.02.003.

[19] J. Li, X. Meng, L. Wan, and Y. Huang, 'Welding of high entropy alloys: Progresses, challenges and perspectives', *Journal of Manufacturing Processes*, vol. 68, pp. 293–331, Aug. 2021, doi: 10.1016/j.jmapro.2021.05.042.

[20] A. O'Brien and C. Guzman, Eds., *Welding handbook. Vol. 3: Welding processes, part 2 / Annette O'Brien, ed*, 9. ed., vol. 3. Miami, Fla: American Welding Soc, 2007.

[21] C. L. Jenney, A. O'Brien, American Welding Society, and Welding Handbook Committee, Eds., *Welding handbook*, 9th ed. Miami, FL: American Welding Society, 2001.

[22] N. F. Kazakov, Ed., *Diffusion bonding of materials*, 1st ed. Oxford [Oxfordshire] ; New York : Moscow: Pergamon Press ; Mir Publishers, 1985.

[23] M. V. V. Mortean, L. H. R. Cisterna, K. V. Paiva, and M. B. H. Mantelli, 'Development of diffusion welded compact heat exchanger technology', *Applied Thermal Engineering*, vol. 93, pp. 995–1005, Jan. 2016, doi: 10.1016/j.applthermaleng.2015.09.021.

[24] S.-X. Li, F.-Z. Xuan, S.-T. Tu, and S.-R. Yu, 'Microstructure evolution and interfacial failure mechanism in 316LSS diffusion-bonded joints', *Materials Science and Engineering: A*, vol. 491, no. 1–2, pp. 488–491, Sep. 2008, doi: 10.1016/j.msea.2008.02.037.

[25] L. B. Mateus *et al.*, '316L Stainless Steel Diffusion Bonding Optimized Parameters', in *Procceedings of the 24th ABCM International Congress of Mechanicl Engineering*, ABCM, 2017. doi: 10.26678/ABCM.COBEM2017.COB17-2078.

[26] T. Song, X. Jiang, Z. Shao, D. Mo, D. Zhu, and M. Zhu, 'The Interfacial Microstructure and Mechanical Properties of Diffusion-Bonded Joints of 316L Stainless Steel and the 4J29 Kovar Alloy Using Nickel as an Interlayer', *Metals*, vol. 6, no. 11, p. 263, Nov. 2016, doi: 10.3390/met6110263.

[27] Y. J. Fang, X. S. Jiang, D. F. Mo, T. F. Song, and Z. P. Luo, 'Microstructure and mechanical properties of the vacuum diffusion bonding joints of 4J29 kovar alloy and 316L stainless steel using pure cobalt interlayer', *Vacuum*, vol. 168, p. 108847, Oct. 2019, doi: 10.1016/j.vacuum.2019.108847.

[28] Y. Liu, 'Interfacial Behavior and Joint Performance of High-entropy Alloy CoCrFeMnNi and Pure Cu Joints Obtained by Vacuum Diffusion Welding', *JME*, vol. 53, no. 2, p. 84, 2017, doi: 10.3901/JME.2017.02.084.

[29] S. Li *et al.*, 'Microstructure and Mechanical Properties of Diffusion-Bonded CoCrNi-Based Medium-Entropy Alloy to DD5 Single-Crystal Superalloy Joint', *Crystals*, vol. 11, no. 9, p. 1127, Sep. 2021, doi: 10.3390/cryst11091127.

[30] M. Samiuddin, J. Li, A. D. Chandio, M. Muzamil, S. U. Siddiqui, and J. Xiong, 'Diffusion welding of CoCrNi medium entropy alloy (MEA) and SUS 304 stainless steel at different bonding temperatures', *Weld World*, vol. 65, no. 11, pp. 2193–2206, Nov. 2021, doi: 10.1007/s40194-021-01165-5.

[31] M. Samiuddin, J. Li, M. Muzamil, S. Uddin, and J. Xiong, 'Mechanical and Microstructural Characterization of the Bond Interface Formed in Diffusion Welding of CoCrNi Medium Entropy Alloy (MEA) and AISI 304 Stainless Steel Under Various Processing Parameters', *Met. Mater. Int.*, vol. 29, no. 5, pp. 1421–1440, May 2023, doi: 10.1007/s12540-022-01309-2.

[32] H. Sun, N. Hashimoto, and H. Oka, 'Vacuum diffusion bonding between equiatomic CoCrNi-based concentrated solid solution alloys system and 316 stainless steel by spark plasma sintering', *Materials Science and Engineering: A*, vol. 879, p. 145297, Jul. 2023, doi: 10.1016/j.msea.2023.145297.

[33] A. Berger, S. Benito, A. Konchits, G. Laplanche, B. Shanina, and S. Weber, 'Thermophysical properties of equiatomic CrMnFeCoNi, CrFeCoNi, CrCoNi, and CrFeNi high- and medium-entropy alloys', *Materials Today Communications*, vol. 39, p. 109341, Jun. 2024, doi: 10.1016/j.mtcomm.2024.109341.

[34] M. C. Harold, Ed., *Steel products manual. Stainless steels*. Warrendale, PA: Iron & Steel Society, 1999.

[35] Z. Wu, H. Bei, F. Otto, G. M. Pharr, and E. P. George, 'Recovery, recrystallization, grain growth and phase stability of a family of FCC-structured multi-component equiatomic solid solution alloys', *Intermetallics*, vol. 46, pp. 131–140, 2014, doi: 10.1016/j.intermet.2013.10.024.

[36] M. Kumaran, T. Sathies, N. S. Balaji, G. Bharathiraja, S. Mohan, and V. Senthilkumar, 'Influence of heat treatment on stainless steel 316L alloy fabricated using directed energy deposition', *Materials Today: Proceedings*, vol. 62, pp. 5307–5310, 2022, doi: 10.1016/j.matpr.2022.03.380.

[37] Y.-Y. Tan *et al.*, 'Chemical composition dependent local lattice distortions and magnetism in high entropy alloys', *Intermetallics*, vol. 129, p. 107050, Feb. 2021, doi: 10.1016/j.intermet.2020.107050.

[38] K.-Y. Tsai, M.-H. Tsai, and J.-W. Yeh, 'Sluggish diffusion in Co–Cr–Fe–Mn–Ni high-entropy alloys', vol. 61, no. 2013, pp. 4887–4897, 2013, doi: http://dx.doi.org/10.1016/j.actamat.2013.04.058.
[39] M. Vaidya, K. G. Pradeep, B. S. Murty, G. Wilde, and S. V. Divinski, 'Bulk tracer diffusion in CoCrFeNi and CoCrFeMnNi high entropy alloys', *Acta Materialia*, vol. 146, pp. 211–224, Mar. 2018, doi: 10.1016/j.actamat.2017.12.052.
[40] M. Mohammadzadeh and R. Mohammadzadeh, 'Effect of grain size on apparent diffusivity in nanocrystal α-iron by atomistic simulation', *Computational Materials Science*, vol. 129, pp. 239–246, Mar. 2017, doi: 10.1016/j.commatsci.2016.12.036.
[41] W. D. Callister and D. G. Rethwisch, *Materials science and engineering: an introduction*, 10th ed. USA: Wiley, 2018.
[42] M. Y. Demeri, *Advanced high-strength steels: science, technology, and applications*. Materials Park, Ohio: ASM Internat, 2013.
[43] S.-X. Li, Y.-N. He, S.-R. Yu, and P.-Y. Zhang, 'Evaluation of the effect of grain size on chromium carbide precipitation and intergranular corrosion of 316L stainless steel', *Corrosion Science*, vol. 66, pp. 211–216, Jan. 2013, doi: 10.1016/j.corsci.2012.09.022.

Conflict of Interest

Author names: Olushola. B. Nenuwa, Léo Thiercelin, Laurent Peltier, Eric Fleury, Nathalie Siredey-Schwaller, Adil Benaarbia

Manuscript title: Dissimilar diffusion welding of some equiatomic FCC-structured CoCrFeNibased binary and multi-component alloys to 316L stainless steel

I (Adil Benaarbia) write on behalf of myself and all co-authors to confirm that the results reported in the manuscript are original and neither the entire work, nor any of its parts have been previously published. The authors confirm that the article has not been submitted to peer review, nor has been accepted for publishing in another journal. The authors confirm that the research in their work is original, and that all the data given in the article are real and authentic. If necessary, the article can be recalled, and errors corrected.

Also, there is no conflict of interest.

Declaration of Interest Statement

Author names: Olushola. B. Nenuwa, Léo Thiercelin, Laurent Peltier, Eric Fleury, Nathalie Siredey-Schwaller, Adil Benaarbia

Manuscript title: Dissimilar diffusion welding of some equiatomic FCC-structured CoCrFeNi based binary and multi-component alloys to 316L stainless steel

The authors declare that they have no known competing financial interests or personal relationships that could have appeared to influence the work reported in this article.

Highlights

- A thorough investigation was carried out to assess the joint integrity of dissimilar diffusion welding of some equiatomic binary and multi-component alloys to 316L stainless steel.
- The microstructures and chemical gradients at the bond interfaces were examined by SEM-EDS, EBSD and XRD analyses, while the mechanical properties were assessed by shear tests.
- The binary and multi-component alloys were successfully joined to SS316L with low interfacial defects and without any compositional segregation or formation of secondary intermetallic compounds at the bond interfaces.
- The shear tests revealed that SS316L-CoCrNi and SS316L-CoCrFeNi joints offered good shear strength and ductility which are comparable to that of SS316L similar joints.